Univerza v Ljubljani
Institut "Jožef Stefan" , Ljubljana
61 111 Ljubljana, Jamova 39, pp 100 / Tel:+386 61 177 3900 / Fax: +386 61 125 7074

IJS Report
IJS - DP - 8113
August 1999

Alignment of RICH and ECAL with data

M. Starič and P. Križan
"J. Stefan" Institute and University of Ljubljana, Ljubljana, Slovenia

Abstract

A subset of data recorded without magnetic field were used to align the optical system of the HERA-B RICH counter relative to the electromagnetic calorimeter.

1 Introduction

With the data recorded without the magnetic field, an alignment method became possible that very closely resembles the method developed on simulated data by at A. Gorišek in his diploma thesis [1]. Some modifications were necessary, in particular since in the original version a full track information was assumed, while presently track candidates are given by high energy clusters in the calorimeter.

In a precursor study [2] it was shown that the high energy calorimeter clusters, as identified in the calorimeter, do indeed provide a useful track direction information if combined with the information on the average interaction point position (Fig. 1). The present study

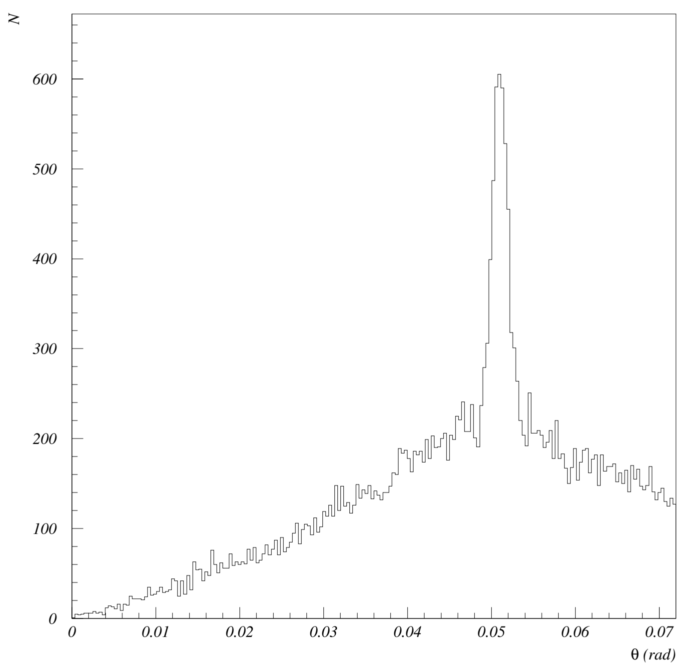

Figure 1: Measured Čerenkov angle ϑ_c relative to track candidate direction as given by the cluster position, with cluster energy restricted to values higher than 10 GeV [2]. The peak at the so called saturated value, characteristic for $\beta = 1$ particles, corresponds to Čerenkov photons of real electrons or positrons.

was motivated by the relative misalignment of the calorimeter and RICH as noticed already in [2] and [3]. The data also indicated that the alignment is different for the upper and for the lower photon detector [2], but no systematic effect could be traced to be the reason for it. Clearly, a finer granularity than detector half is needed for studies of systematic effects, and the natural unit is the separation of hits on the photon detector according to the pairs of spherical and planar mirror segments from which they were unambiguously reflected.

In the report we shall first briefly discuss the data used, and then explain in some detail the method employed for the determination of Čerenkov angle for $\beta = 1$ particles, the extraction of alignment parameters for each spherical - planar mirror combination, as well as the solution of the resulting system of linear equations. Finally, the results will be presented: the comparison of Čerenkov angle resolution prior and after the realignment, as well as the alignment parameters for individual mirror segments. At the end we shall investigate possible systematic errors of the method by analysing various sets of data with two different radiator gases, different wire targets, data recorded with magnetic field, as well as simulated data.

2 Data selection and handling

Data used are from a particular run 4026, recorded on March 25, 1999. To simplify the transport, and subsequent handling, only raw RICH information (FED buffer) was written to an output file together with the ECAL cluster data. A sample of 65k events is in this form stored in a file of 279 Mbytes. The results were checked by an analysis of a larger data sample (runs 4393 and 4424), a sample recorded with nitrogen as radiator gas without magnetic field (run 1335), on data with magnetic field turned on (runs 5488, 5490, 5522) as well as on simulated data.

The geometrical constants were taken from the official ARTE tables. No shifts of detector elements relative to the values given there were made.

Run number	events	radiator	mag. field	target wire	vertex position (mm)	trigger
4026	107k	freon	off	Inner II	(2,0,-47)	pretr., FLTE
4393, 4424	585k	freon	off	Inner II	(2,0,-47)	pretr., FLTE
1335	29k	nitrogen	off	Inner II	(2,0,-47)	min.bias
5488, 5490	120k	freon	on	Inner II	(2,0,-47)	pretr., FLTE
5522	159k	freon	on	Below I, Inner I	(1,-1,-8.5)	pretr., FLTE

3 The method

Čerenkov photons that are emitted from a single track, are distributed on the detector area over a slightly distorted ring. The center of the ring is given by the track direction, which is, in turn, measured by a tracking system. If the mirror segments and the tracking system are not aligned perfectly, the centre of the observed photon ring will not coincide with the expected centre, the point which is determined by the charged particle direction vector reflected on the mirrors in ideal positions. The measured Čerenkov angle (ϑ_c), the angle between the direction defined by the photon hit on the photon detector and the direction defined by the particle path reflected on ideally positioned mirrors (point C on Fig. 2), corresponds to the ring radius. As a result the ring center displacements, the measured value of the Čerenkov angle becomes dependent on the azimuthal angle around track direction (Fig. 3). For small displacements from the expected position, this variation can be written as

$$\vartheta_c = \vartheta_0 + \Delta\phi \cos\varphi_c + \Delta\lambda \sin\varphi_c, \quad (1)$$

where $\Delta\phi$ and $\Delta\lambda$ stand for the displacements of the mirror in the ϕ and λ coordinates (very roughly corresponding to a rotation in the horizontal and vertical plane, respectively [4]). It is the aim of the alignment procedure to determine the two angular displacements $\Delta\phi$ and $\Delta\lambda$.

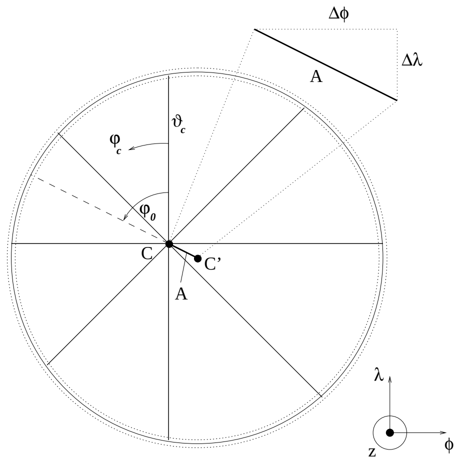

Figure 2: Čerenkov ring. The point C stands for the expected position of the ring centre given by the particle trajectory, and C' is the actual centre of the ring as obtained in case of a relative misalignment of the tracking system and the mirrors [1].

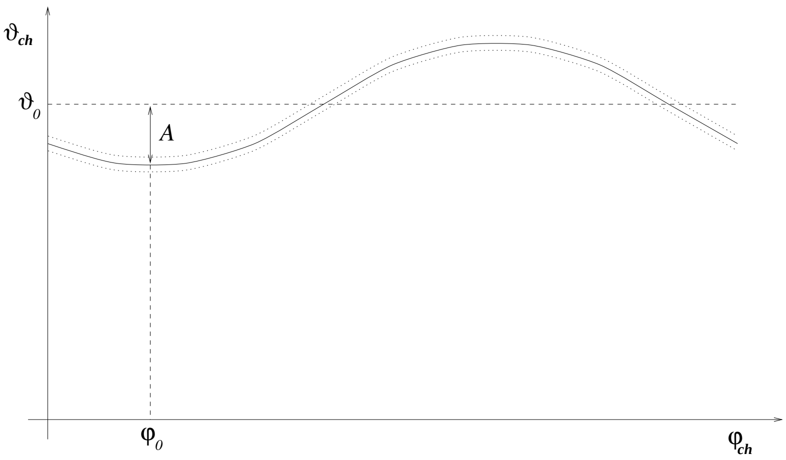

Figure 3: Measured Čerenkov angle ϑ_c as a function of φ_c in case of a misaligned mirror [1].

In the absence of magnetic field, the direction of the track candidate is determined from the coordinates of the corresponding cluster in the shower counter and from the wire target position. In order to exclude the contribution from multiple scattering of electrons to the Čerenkov angle resolution, we have restricted our analysis only to clusters with the energy above 5 GeV.

3.1 Unambiguous photons

An essential feature of the method employed in this analysis is the use of photons for which we can unambiguously determine from which spherical and planar mirror segments it was reflected. Such photons (Fig. 4) we shall call unambiguous photons. The procedure for the

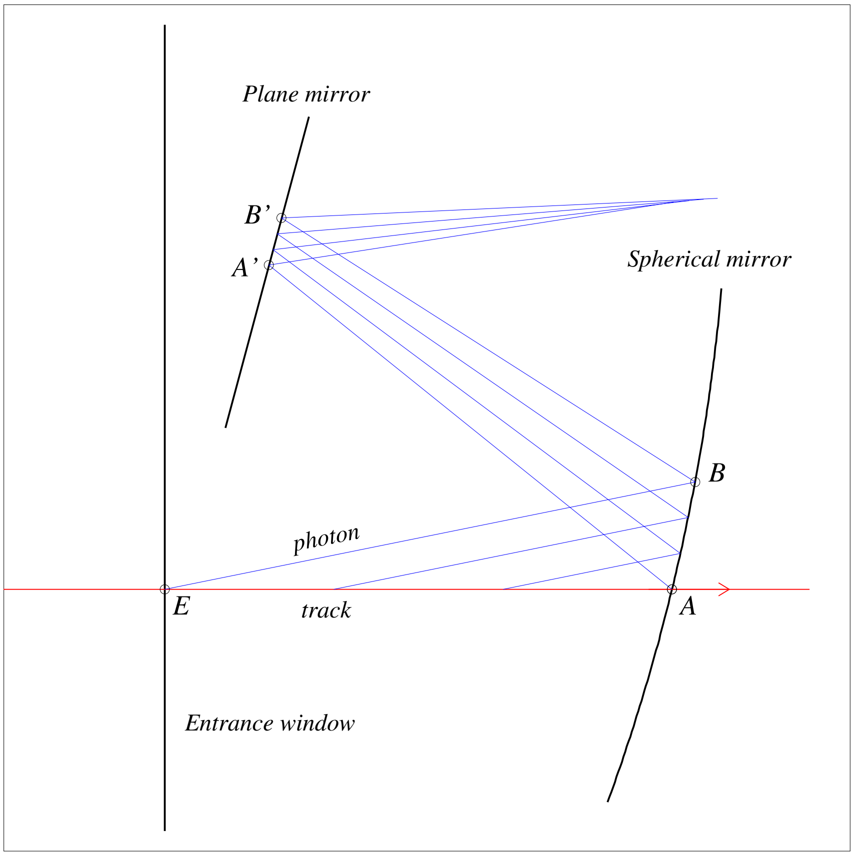

Figure 4: Unambiguous photons: a hit corresponds to an unambiguous photon of a given track if both the photon emitted in point E and the photon emitted in point A get reflected from the same combination of spherical and planar mirrors.

determination of whether a photon is unambiguous or not is as follows. After reconstructing the direction of the photon (i.e. by determining its λ and ϕ) for a given hit-track pair, we perform two ray tracings: from point E and from point A (Fig. 4). The photon is unambiguous, if the points A and B are on the same spherical mirror, and points A' and B' are on the same planar mirror.

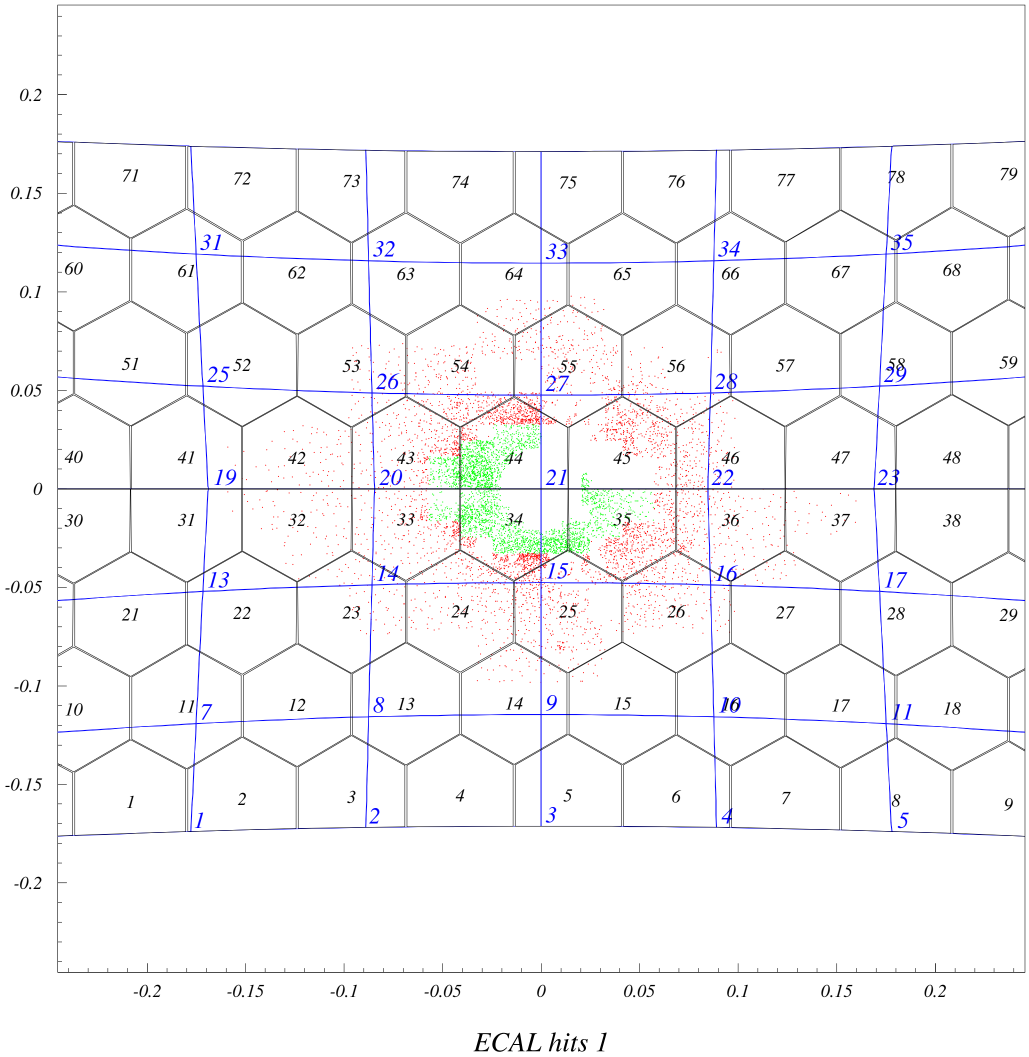

Figure 5: The system of mirrors in the HERA-B RICH in the angular space $t_x = x_{clus}/z_{clus}$ and $t_y = y_{clus}/z_{clus}$. Indices of spherical mirrors are given in the middle of the segment, of the planar ones in the lower left corner. Note that the usual two index (row, column) description of mirrors is related to the above indexing in the following way: planar mirror index = 6·row + column, spherical mirror index = 10·row + column. Also shown is the distribution of hits on the calorimeter for the run 4026.

3.2 Čerenkov angle as a function of the azimuthal angle around track direction

To determine the parameters $\Delta\phi$ and $\Delta\lambda$ for a particular combination of spherical and planar mirror segments, we first fill the histogram of Čerenkov angle versus the azimuthal angle around track direction by using unambiguous photons reflected from this pair of mirror segments. As can be seen from the left side of Fig. 6, the variation follows the expected function at least qualitatively. To quantify the agreement, we have in each of the 50 intervals in φ_c fitted a Gaussian function and a second order polynomial over an interval $\vartheta_c = 0.040$ to $\vartheta_c = 0.060$ (Fig. 7). All parameters were left to vary freely. To get an impression on the fit quality, we plot in Fig. 9 the resulting distribution of χ^2, which looks reasonable. It is also instructive to plot the distribution of the fitted value of the peak r.m.s. width (Fig. 8).

If we then plot the resulting peak position as a function of φ_c (right side of Fig. 6), the sine variation becomes even more apparent.

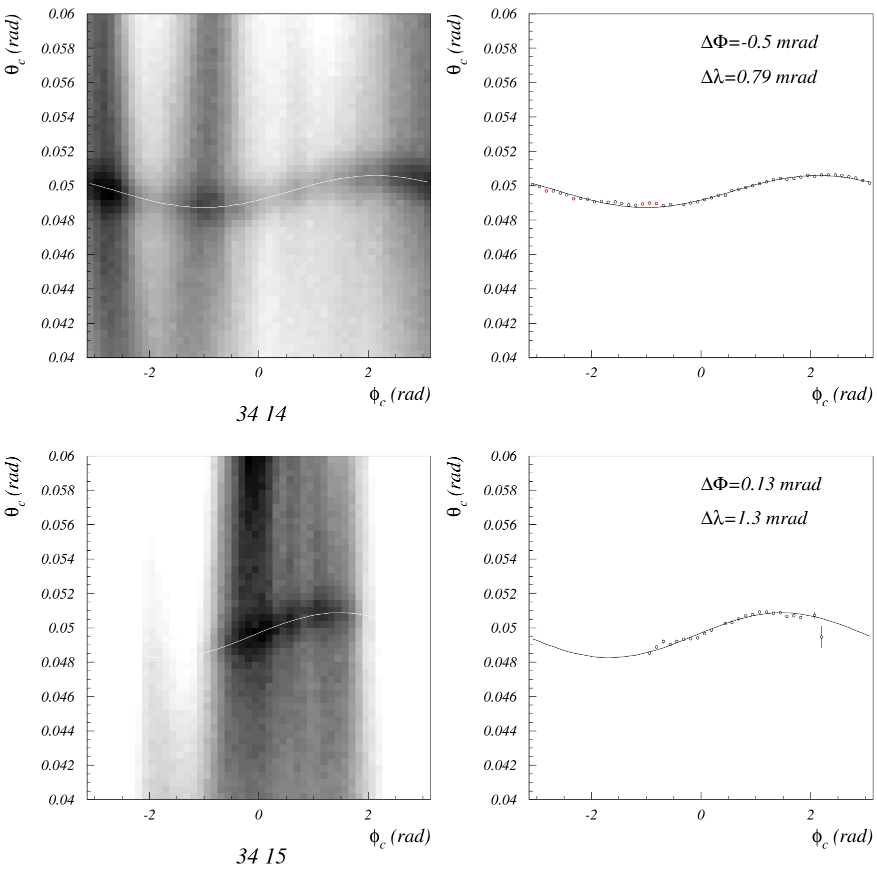

Figure 6: Distribution of hits in the ϑ_c, φ_c plane for two combinations of a spherical (34) and two planar mirror segments (14 and 15). Raw data are shown on the left side, and the saturated ring peak position from the fit in each φ_c slice is shown on the right.

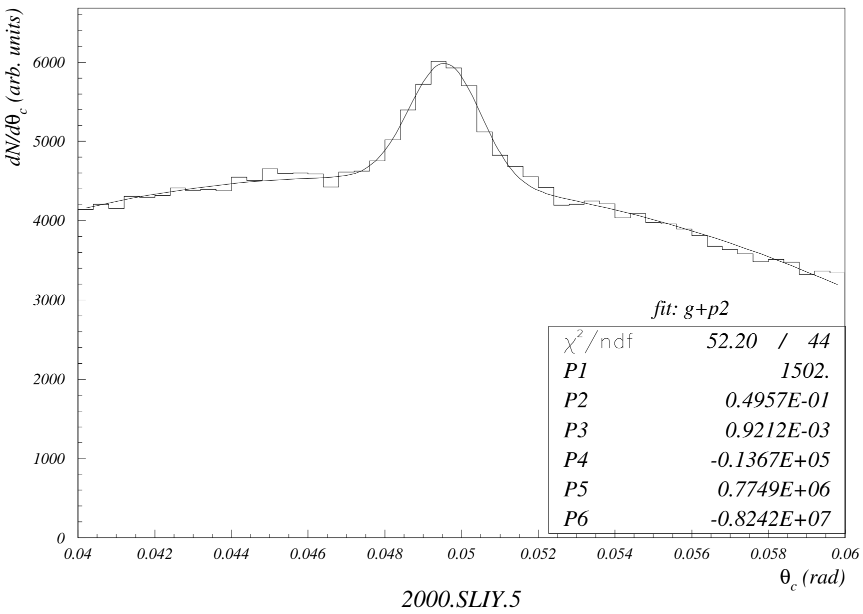

Figure 7: Distribution of hits over ϑ_c in one of the φ_c slices. The result of the fit is superimposed.

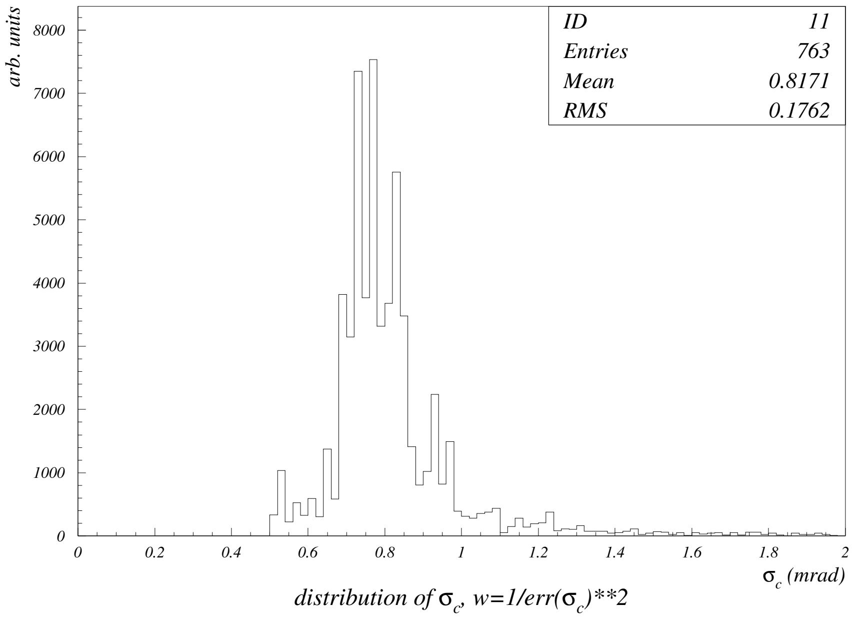

Figure 8: Distribution of the width σ of the saturated peak from the fits to slices in ϑ_c, for all mirror segment pairs studied. Each entry is weighted according to the error in the width value as given by the fit.

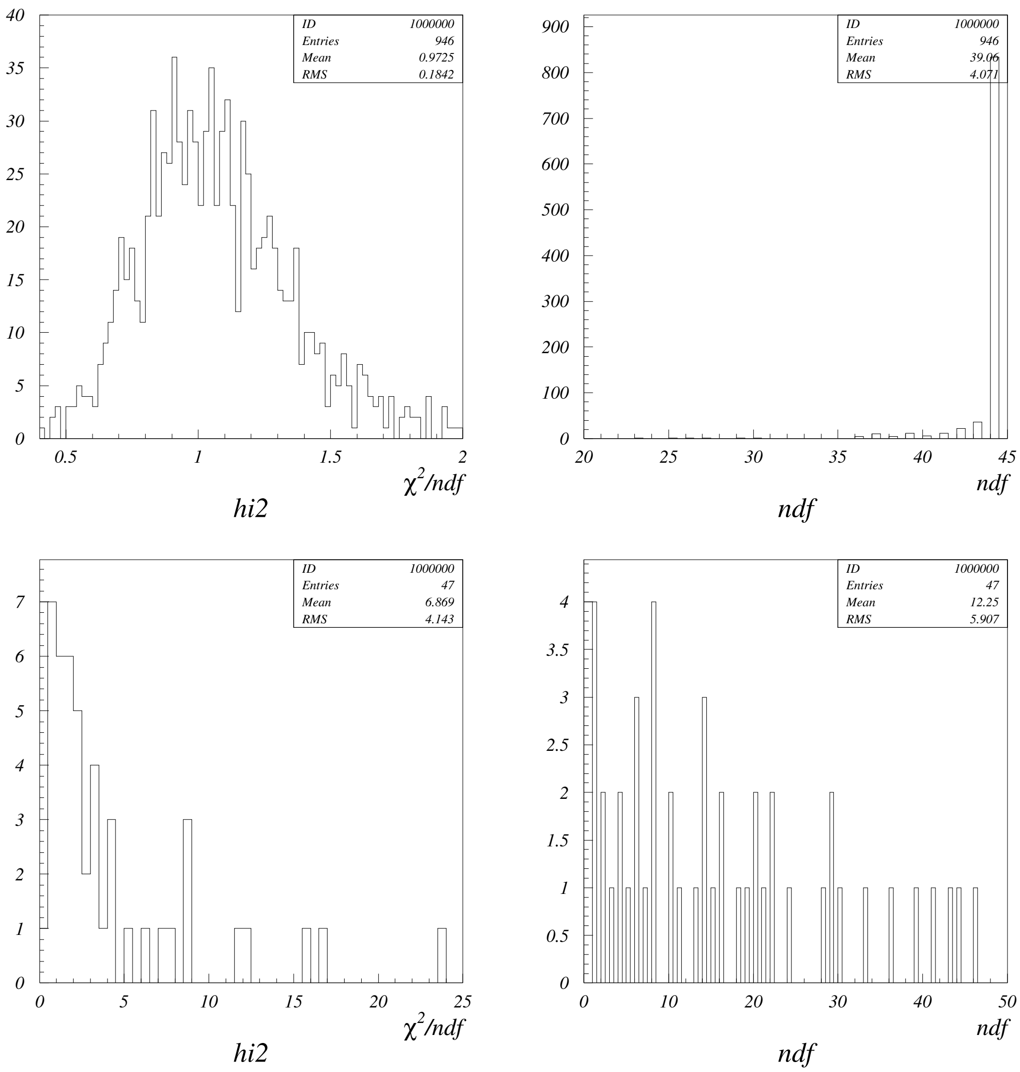

Figure 9: Distribution of $\chi^2/n.d.f.$ and the number of degrees of freedom for fits to distributions in φ_c slices (top), and for fits of the sine modulation in ϑ_c vs. φ_c (bottom).

3.3 Mirror pair direction parameters

Using the ansatz $\vartheta_c = \vartheta_0 + \Delta\phi \cos\varphi_c + \Delta\lambda \sin\varphi_c$, we fitted the measured sine modulation of the Čerenkov angle as a function of the azimuthal angle around track direction. For cases where more than 75% of the azimuthal angle φ_c was covered by unambiguous photons for a given combination of mirror segments, the fit had three free parameters, ϑ_0, $\Delta\phi$ and $\Delta\lambda$, otherwise we have fixed ϑ_0 to the mean saturated Čerenkov angle. The results of the fits are shown in Fig. 10. We note that the distribution over $\chi^2/n.d.f.$ (bottom plots in Fig. 9) indicates that the errors in peak position as given by the fit to φ_c slices are somewhat underestimated.

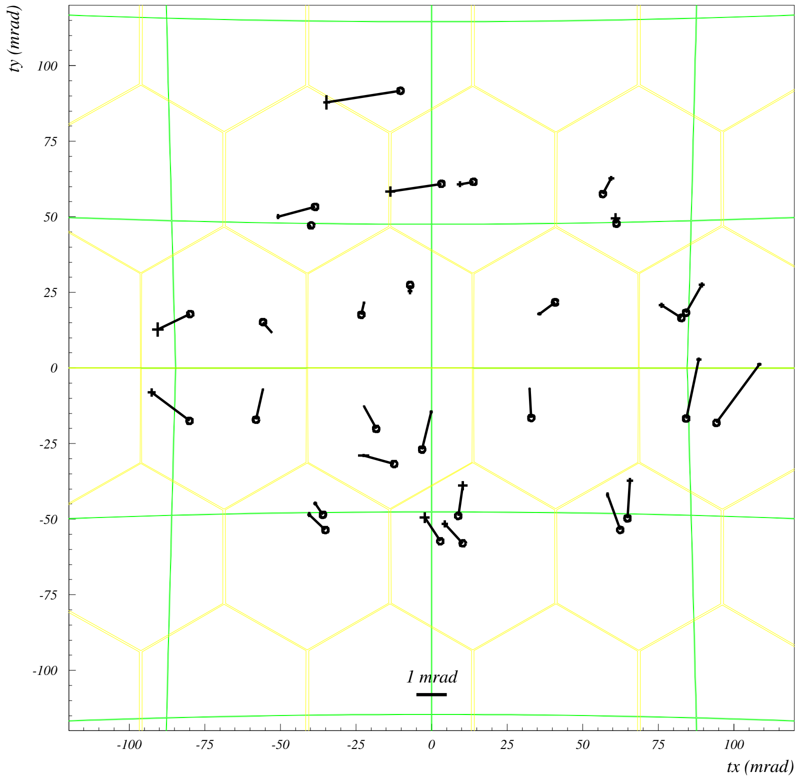

Figure 10: Alignment of combinations of spherical and planar mirror segment pairs relative to the calorimeter given track directions: displacement of each combination is indicated by an arrow originating in the center of gravity of tracks for the given combination. The arrows with different directions can have close origins: this just means that part of the ring is reflected by one and the rest by another spherical–planar mirror combination. The data are from run 4026, target wire Inner II.

3.4 The system of linear equations

For each pair of overlapping spherical (k) and planar (j) mirror segments, each of which contributes to the ring center displacements by $\Delta\phi_k^{sph}$, $\Delta\lambda_k^{sph}$, $\Delta\phi_j^{pl}$, $\Delta\lambda_j^{pl}$, we measure the sum of the two contributions,

$$\Delta\phi_{kj} = \Delta\phi_k^{sph} + \Delta\phi_j^{pl}, \tag{2}$$

$$\Delta\lambda_{kj} = \Delta\lambda_k^{sph} + \Delta\lambda_j^{pl}. \tag{3}$$

By including all k, j pairs with sufficient overlap we arrive at a system of equations. The contributions $\Delta\phi_k^{sph}$, $\Delta\lambda_k^{sph}$, $\Delta\phi_j^{pl}$, $\Delta\lambda_j^{pl}$ are of course related to the unknown mirror alignment parameters, the angular displacements $\Delta\vartheta_x$ and $\Delta\vartheta_y$,

$$\Delta\phi_k^{sph} \approx 2\Delta\vartheta_x^k, \tag{4}$$

$$\Delta\lambda_k^{sph} \approx 2\Delta\vartheta_y^k, \tag{5}$$

$$\Delta\phi_j^{pl} \approx \Delta\vartheta_x^j, \tag{6}$$

$$\Delta\lambda_j^{pl} \approx \Delta\vartheta_y^j. \tag{7}$$

Collecting all n unknowns in a vector $\mathbf{u}$, and all m measured ring displacements $\Delta\phi_{kj}$ and $\Delta\lambda_{kj}$ in a vector $\mathbf{b}$, the above system of equations can be rewritten as

$$\sum_{l=1}^{n} A_{il} u_l = b_i \tag{8}$$

Since each of the planar mirror segments overlaps with several spherical segments, and vice versa, the number (m) of equations (measured deviations) exceeds the number (n) of unknowns (mirror displacements). Note that we have to add an additional condition to fully determine the system: if all spherical mirrors are turned by δ, and all planar mirrors by -2δ, one arrives at the same ring displacements (vector $\mathbf{b}$). Rather than fixing the displacements of one of the mirrors in the lower and one in the upper half to zero (one of the possibilities), we require for the solution to minimize the necessary mirror readjustments,

$$\sum_{l=1}^{n} u_l^2 = min. \tag{9}$$

It is easy to see that this requirement, in turn, results in an additional linear equation,

$$\sum_{is} u_{is} - \sum_{ip} u_{ip} = 0, \tag{10}$$

where the first sum goes over all spherical mirror segment and the second over all planar ones.

The resulting system, Eqs. 8 and 10, is solved by requiring that the properly weighted sum of squares of deviations of the left hand side from the right hand side for the whole system is minimal.

$$\sum_{i=1}^{m} \frac{(\sum_{l=1}^{n} A_{il} u_l - b_i)^2}{\sigma_i^2} = min, \tag{11}$$

where the terms are weighted by the inverse of the error σ_i in measurement of b_i. The resulting linear system,

$$\sum_{l=1}^{n}\sum_{i=1}^{m}\frac{A_{il}A_{ij}}{\sigma_i^2}u_l = \sum_{i=1}^{m}\frac{A_{ij}}{\sigma_i^2}b_i \tag{12}$$

is, of course, similar to the one shown in Ref. [1]. To calculate the solution, we define for the sake of simplicity a new matrix

$$B_{ij} = \sum_{i=1}^{m}\frac{A_{il}A_{ij}}{\sigma_i^2}. \tag{13}$$

Note that $\mathbf{B}$ is symmetric, such that its inverse $\mathbf{B^{-1}}$ is easy to calculate. The solution can then be written as

$$u_k = \sum_{j=1}^{n}(B^{-1})_{kj}\sum_{i=1}^{m}\frac{A_{ij}}{\sigma_i^2}b_i, \tag{14}$$

while the error is calculated from

$$\sigma_{u_k} = \sum_{i=1}^{m}(\sum_{j=1}^{n}(B^{-1})_{kj}\frac{A_{ij}}{\sigma_i})^2. \tag{15}$$

The consistency of the solution can be checked in Fig. 11, where we compare the measured $\Delta\phi$ and $\Delta\lambda$ with sums of the two contributions, $\Delta\phi_k^{sph} + \Delta\phi_j^{pl}$ and $\Delta\lambda_k^{sph} + \Delta\lambda_j^{pl}$, respectively, as they were determined from the above system of equations.

Finally let us note that instead of Eq. 10, one could introduce a different additional constraint. For each of the detector halves one could add a constant displacement to all spherical mirror segments, and subtract the same value from the planar ones,

$$\Delta\phi_k^{sph} \rightarrow \Delta\phi_k^{sph} + \delta\phi$$

$$\Delta\lambda_k^{sph} \rightarrow \Delta\lambda_k^{sph} + \delta\lambda$$

$$\Delta\phi_k^{pl} \rightarrow \Delta\phi_k^{pl} - \delta\phi$$

$$\Delta\lambda_k^{pl} \rightarrow \Delta\lambda_k^{pl} - \delta\lambda$$

and the result would still be a solution of the linear system, Eq. 12. Figure 15 shows an example of two equivalent solutions.

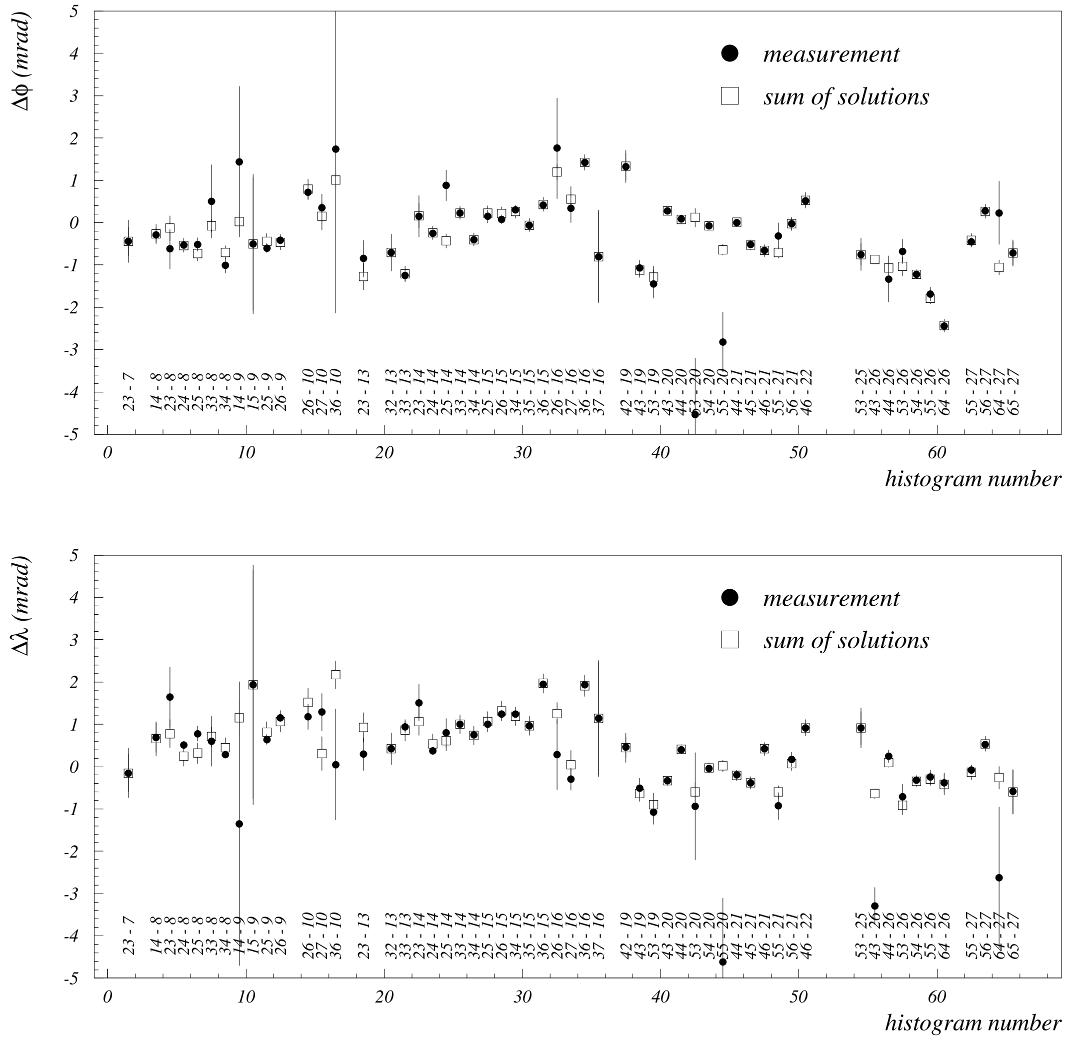

Figure 11: Relative alignment of combinations of spherical and planar mirror segment pairs with respect to the calorimeter given track directions: displacement of each combination of spherical (first index) and planar (second index) mirror segments, as given by the fit to the sine modulation (full circles), and after combining the two displacements, solutions of the system of equations (open circles).

4 Results

4.1 Čerenkov angle resolution

Having solved the system of equations for angular displacements of individual mirror segments, the quality of the new alignment parameters is checked on the data, by examining the Čerenkov angle resolution before and after applying the new alignment parameters, $\Delta\phi_k^{sph}$, $\Delta\lambda_k^{sph}$, $\Delta\phi_j^{pl}$, and $\Delta\lambda_j^{pl}$. The results are shown in Figs. 12 and 13, and summarized in the table below. The method clearly improves the resolution, in some cases quite dramatically.

ECAL-RICH region combination	r.m.s. peak width (mrad) raw data	r.m.s. peak width (mrad) after the correction
inner ECAL, upper M16 RICH	0.87	0.83
inner ECAL, lower M16 RICH	1.16	0.79
middle ECAL, upper M16 RICH	1.35	1.11
middle ECAL, lower M16 RICH	1.55	1.09
middle ECAL, upper M4 RICH	1.42	1.46
middle ECAL, lower M4 RICH	1.91	1.58

4.2 Alignment parameters of individual segments

To examine the size and the nature of the relative misalignments, we first plot the distribution of displacements in the ϕ and λ angle, for the upper and lower planar and spherical mirror segments separately (Fig. 14). To check whether the displacements vary in a systematic way in the vertical or horizontal direction, we plot the displacements as vectors positioned in the middle of each mirror segment (Fig. 15). For the sake of completeness, the same quantity is then shown for a realignment after having applied the calculated realignment rotations in software (Figs. 16).

From the above plots we see a slight systematic effect in the displacement value and direction: the spherical mirrors tend to be turned more to the beam axis, and the planar away from it. Note that the mirrors at the extreme edges of present acceptance have somewhat larger uncertainties in the alignment parameters, and should be taken with caution.

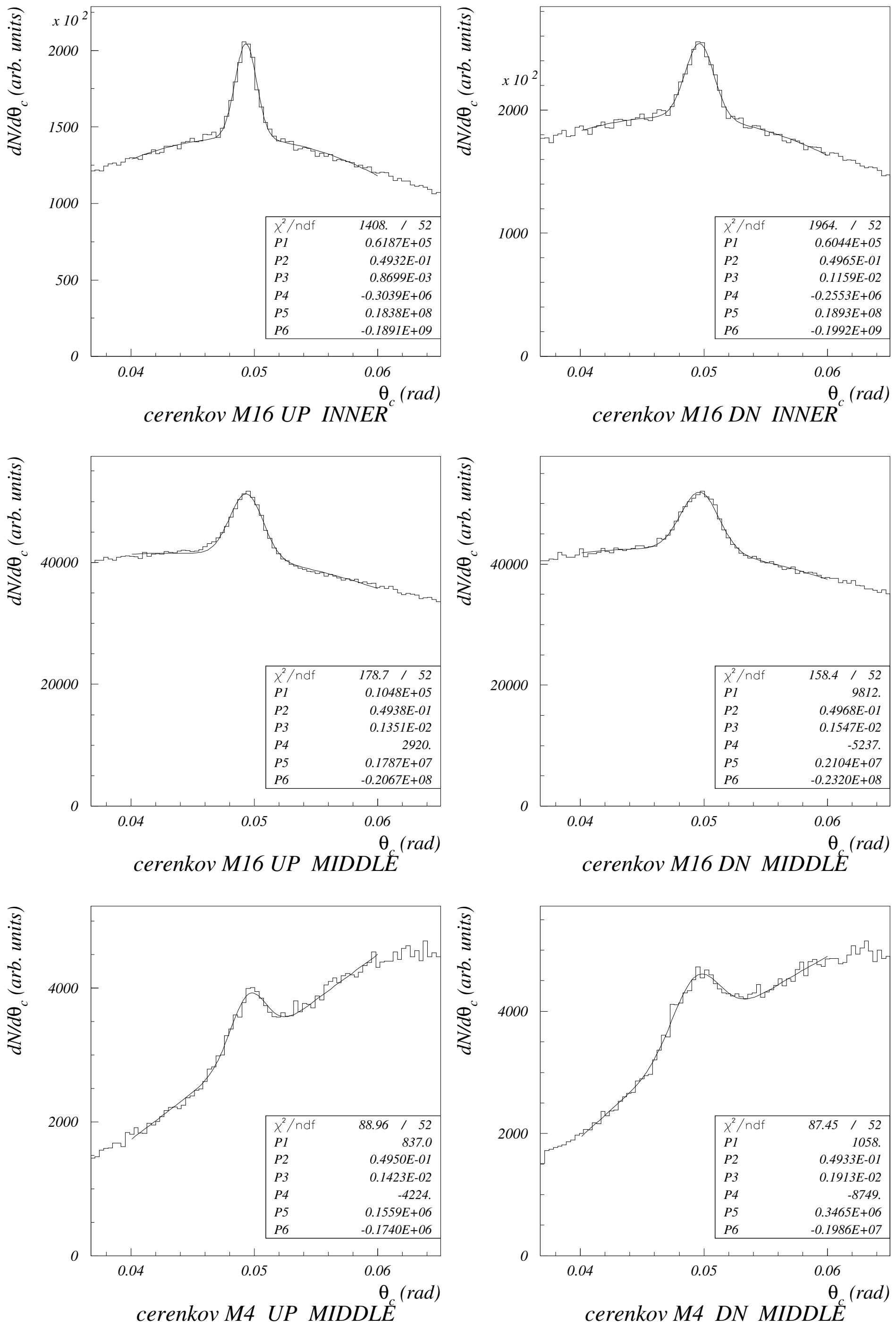

Figure 12: Čerenkov angle distribution for electron candidates for data, i.e. prior applying the alignment corrections, shown separately for the upper and lower photon detector, for the inner and middle calorimeter, and for the M16 and M4 PMT regions.

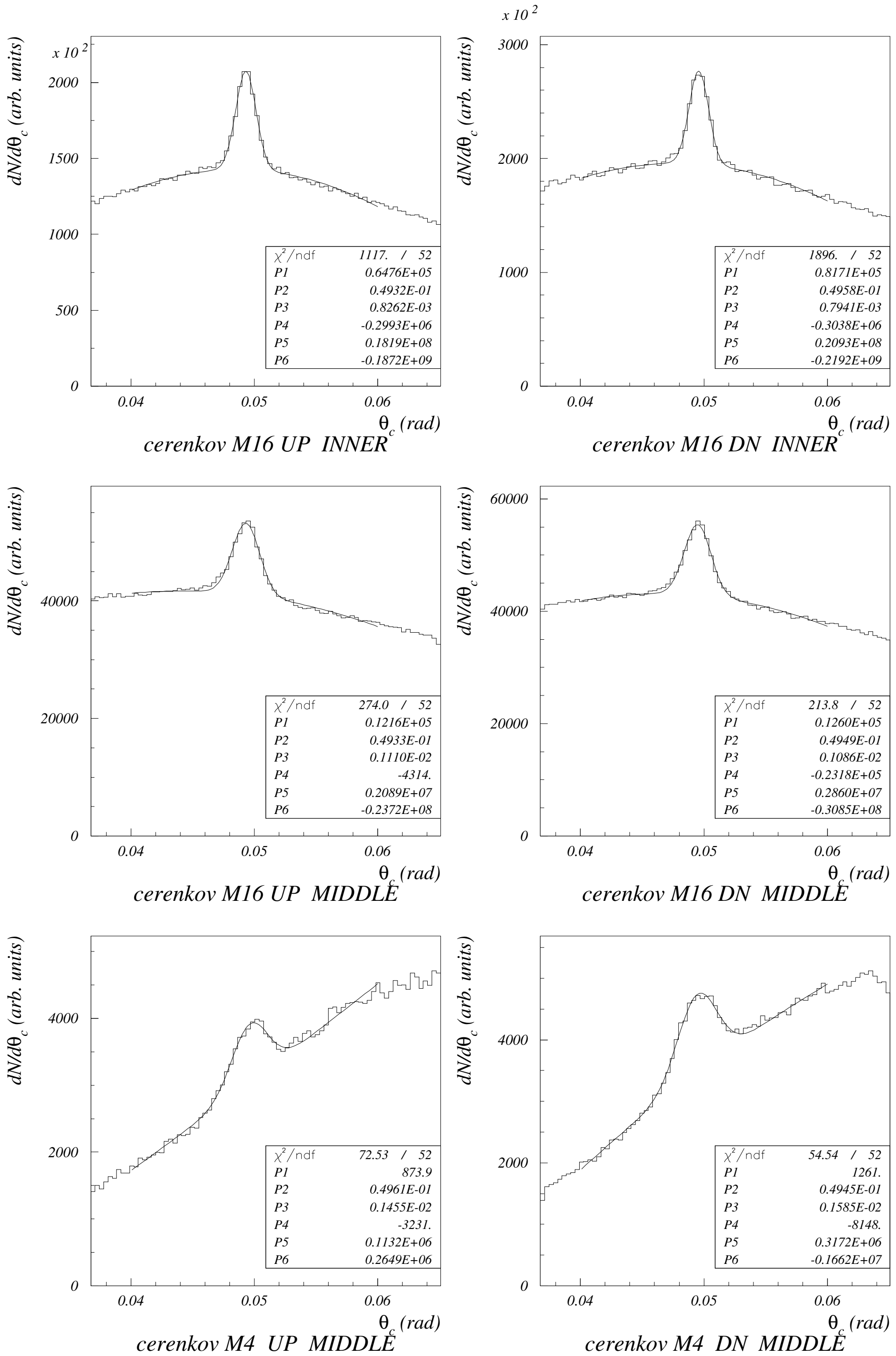

Figure 13: Čerenkov angle distribution for electron candidates after applying the alignment corrections, shown separately for the upper and lower photon detector, for the inner and middle calorimeter, and for the M16 and M4 PMT regions.

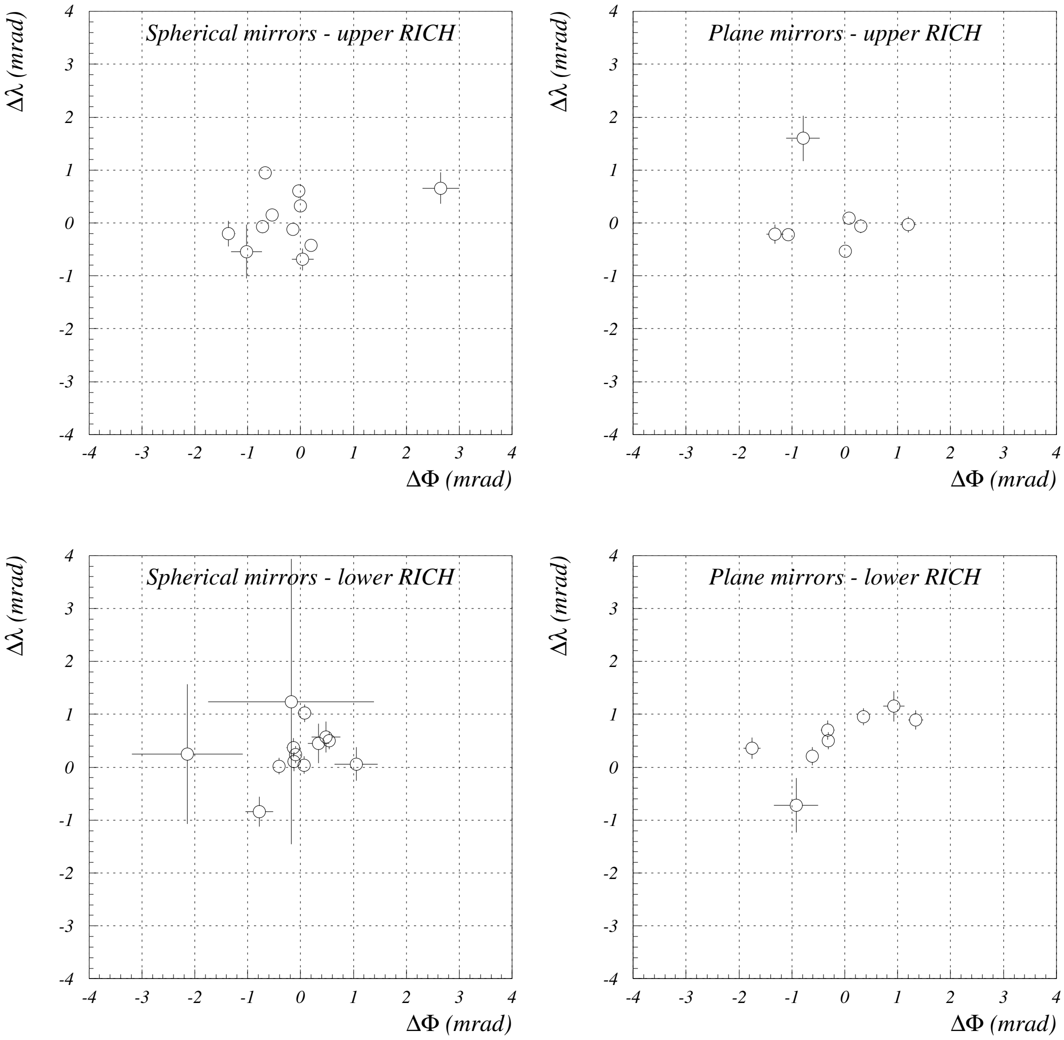

Figure 14: Alignment of spherical and planar mirror segments relative to the calorimeter given track directions: distribution over displacement contributions in the ϕ and λ angle, for the upper and lower planar and spherical mirror segments.

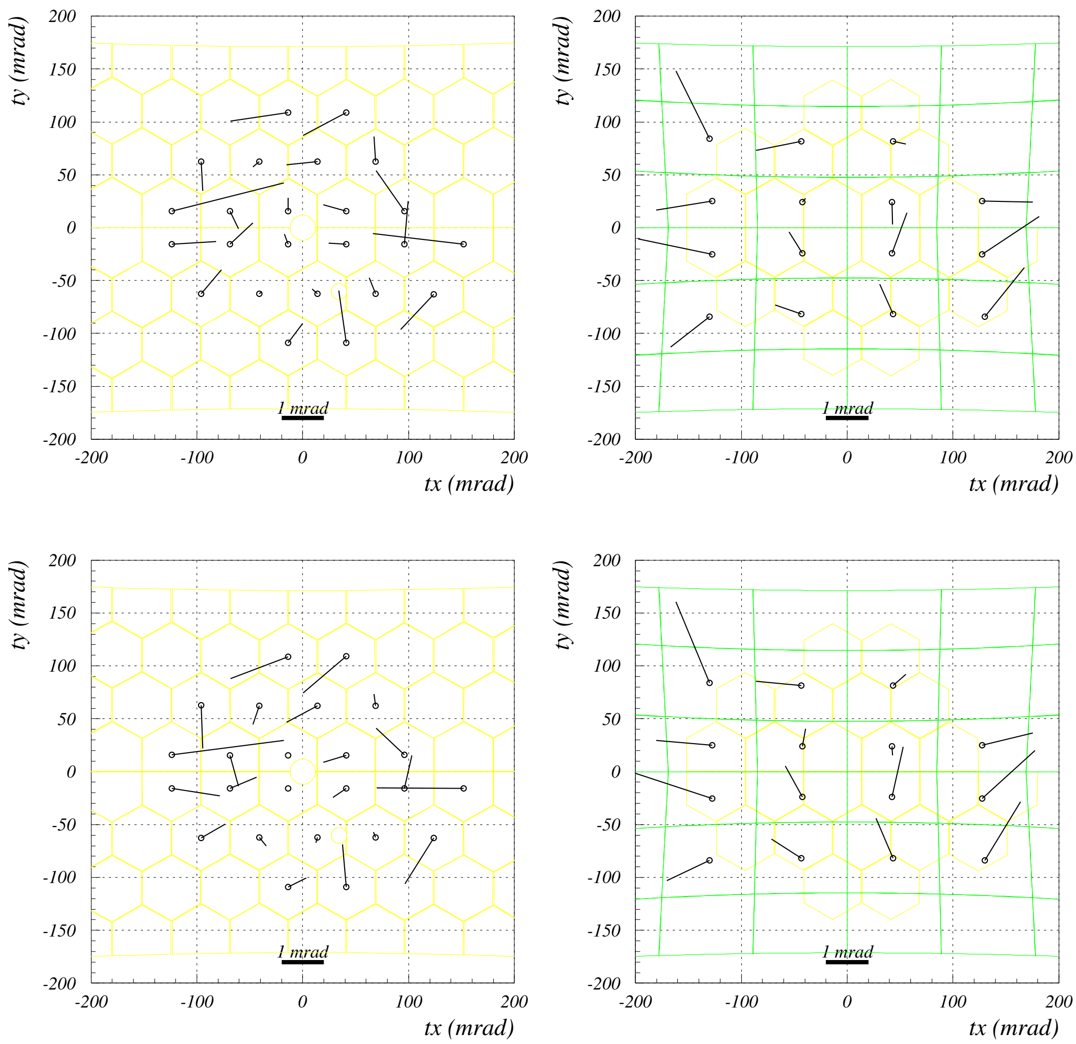

Figure 15: Alignment of spherical (left) and planar (right) mirror segments relative to the calorimeter given track directions: displacement contribution of each mirror segment. Two solutions are shown: one with additional requirement Eq. 9 (top), and another with a fixed spherical mirror segment in each detector half (bottom).

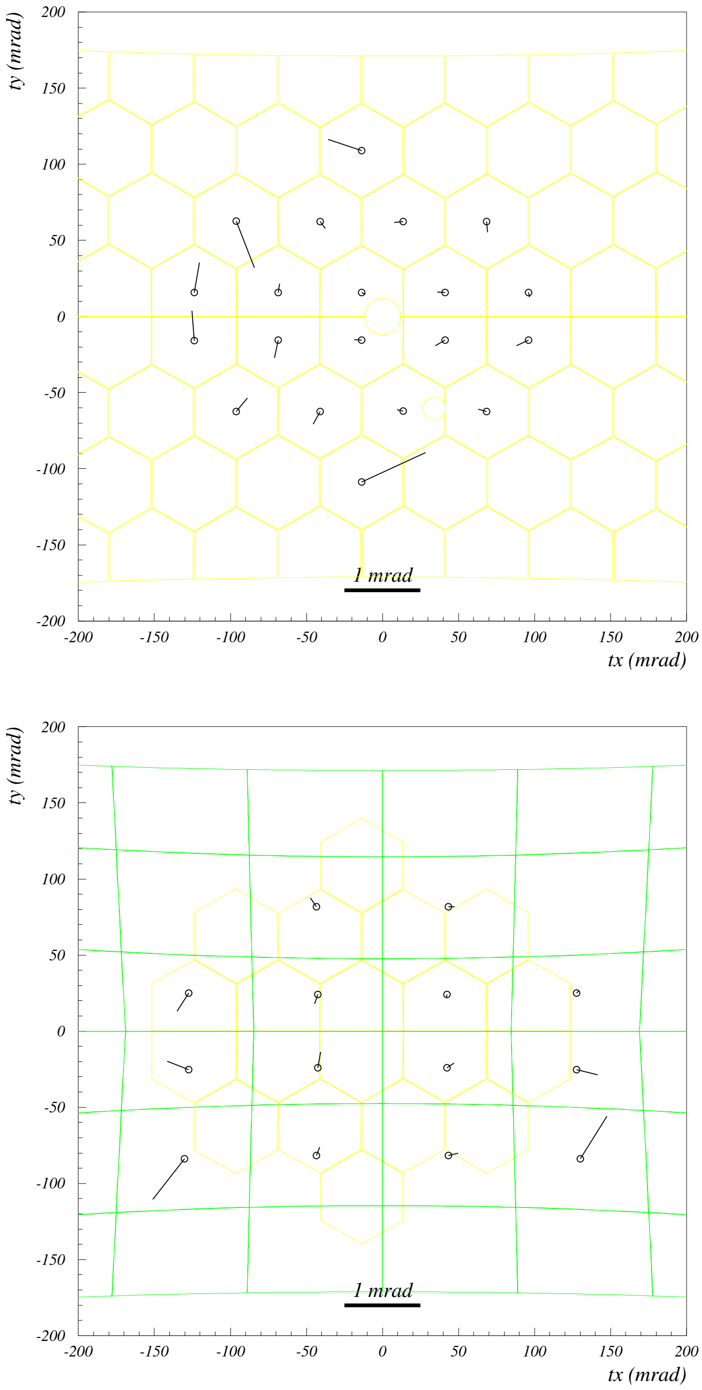

Figure 16: Alignment of spherical (top) and planar mirror (bottom) segments relative to the calorimeter given track directions: displacement contribution of each mirror segment after applying the correction.

5 Analysis of other data sets

To investigate possible systematic effects we have investigated also other data sets, recorded under different conditions. As can be seen from Figs. 17, 18 and 19, there is a good agreement with the results as shown in Fig. 10. This not only shows that the method gives consistent results even for a completely different radiator (nitrogen) with a Čerenkov angle of 25 mrad instead of around 50 mrad, and consequently four times less photons per ring, it also shows that the alignment parameters did not change over an extended period of time (Dec. 98 - April 99).

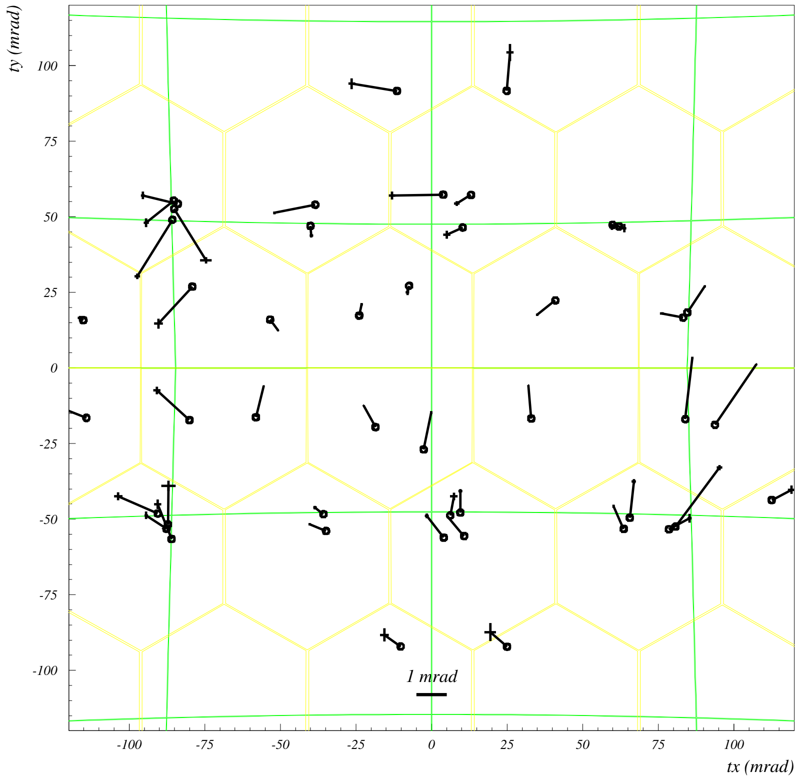

Figure 17: Alignment of the RICH relative to the calorimeter for the runs 4393 and 4424, to be compared with the results for the run 4026, Fig. 10.

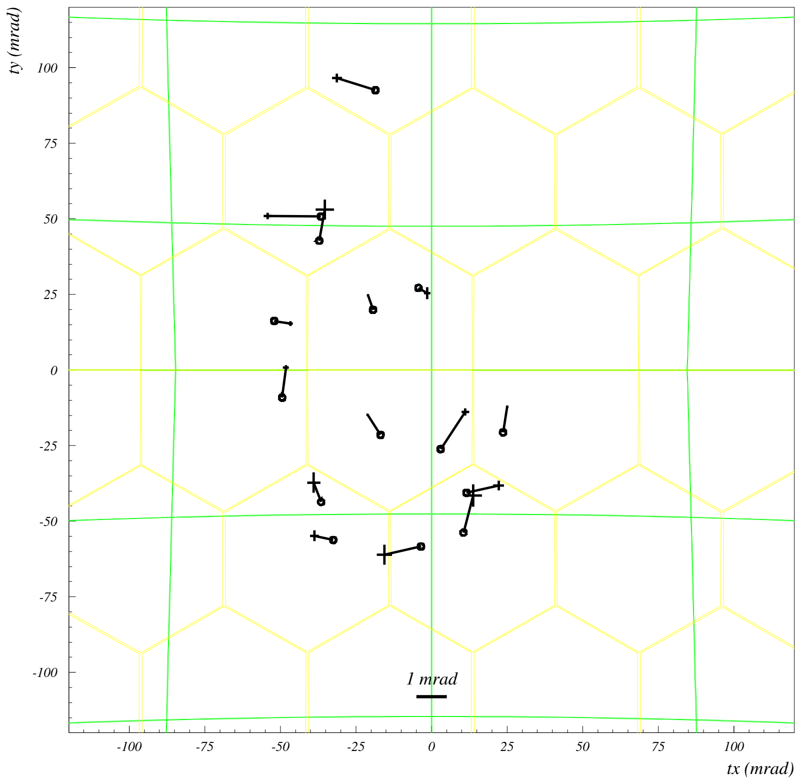

Figure 18: Alignment of the RICH relative to the calorimeter for the run 1335, with nitrogen used as the radiator gas (magnet was off, and the Inner II target was used). Note that due to the fact that there is little data available in the period in question, and the ECAL had less equipped channels on the positive x side, the region where the displacement parameters could be deduced in the given data sample is somewhat restricted.

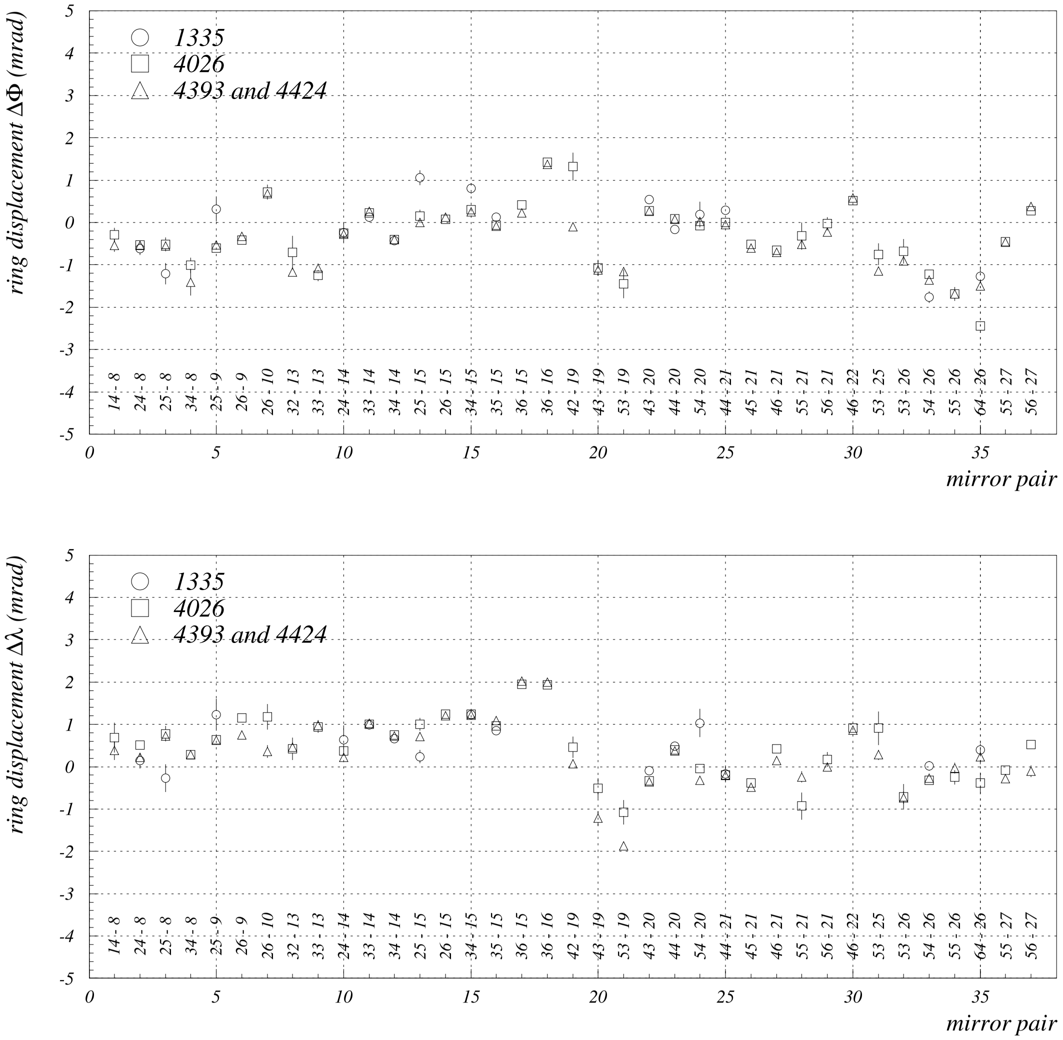

Figure 19: Comparison of results from different data sets: displacement of each combination of spherical (first index) and planar (second index) mirror segments, run 4026 (squares), runs 4393 and 4424 (triangles), run 1335 with nitrogen (circles).

5.1 Analysis of simulated data

Possible systematic effects were also checked by using MC generated data. 64k minimum bias events were generated (target Inner II), and subsequently analysed by using the same program as for the real data. In the simulation all mirror segments were assumed to be perfectly aligned with the calorimeter.

From Figs. 20 and 21 we conclude that we the limited statistics we cannot exclude some small systematic effects (order 0.1 mrad), which are clearly smaller that the effects observed on the real data.

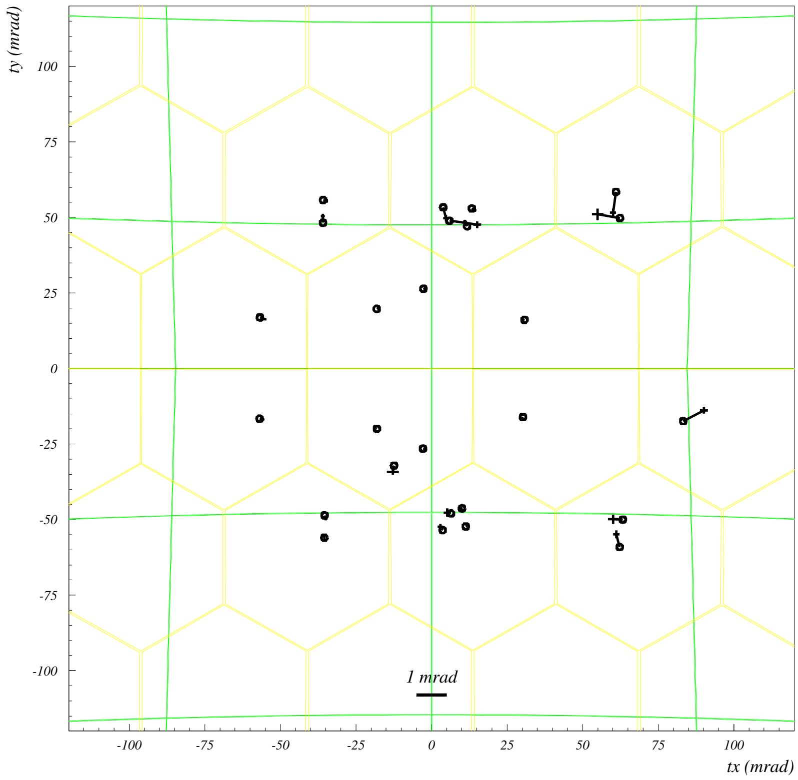

Figure 20: Simulated data: alignment of the RICH relative to the calorimeter. In the simulation all mirror segments were assumed to be perfectly aligned.

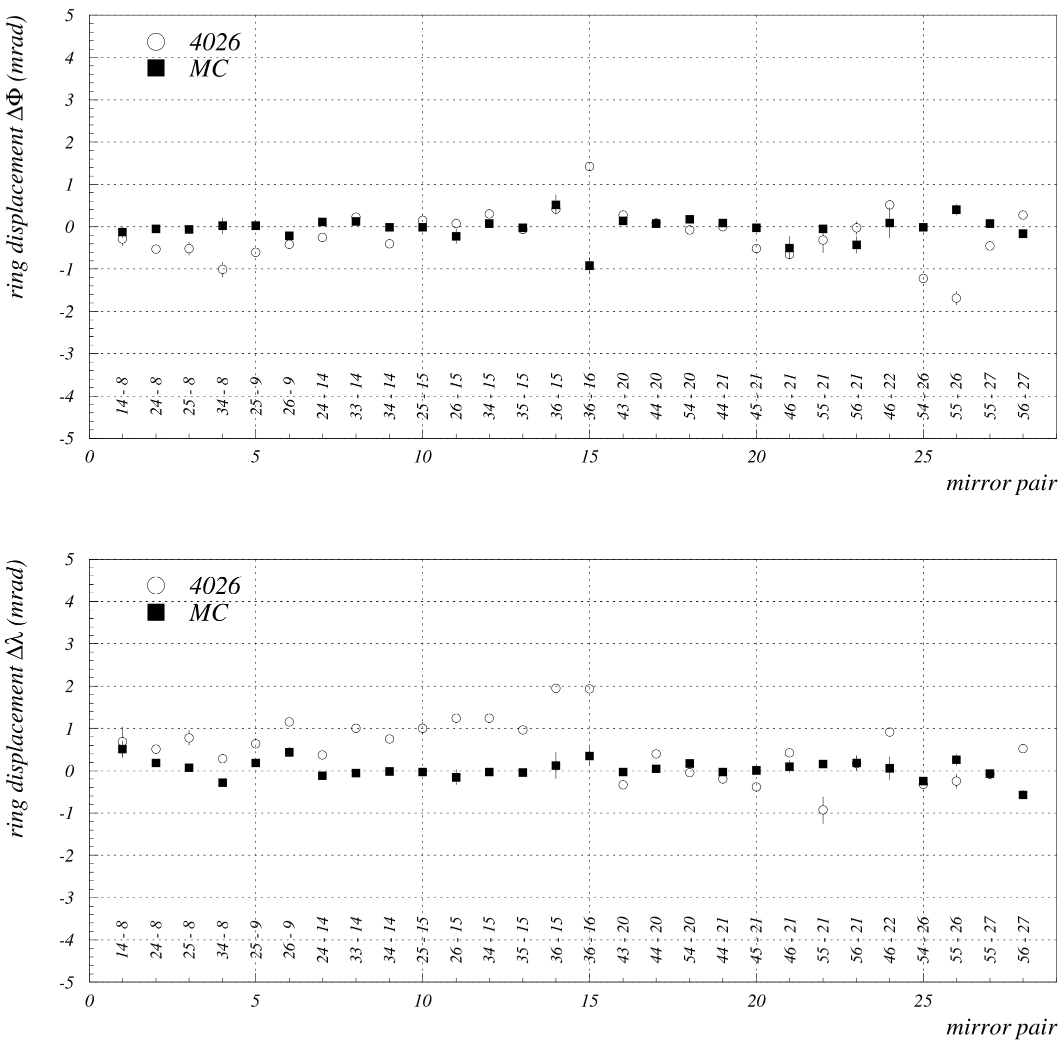

Figure 21: Comparison of results of the analysis of simulated and real data.

5.2 Analysis in the case of magnetic field

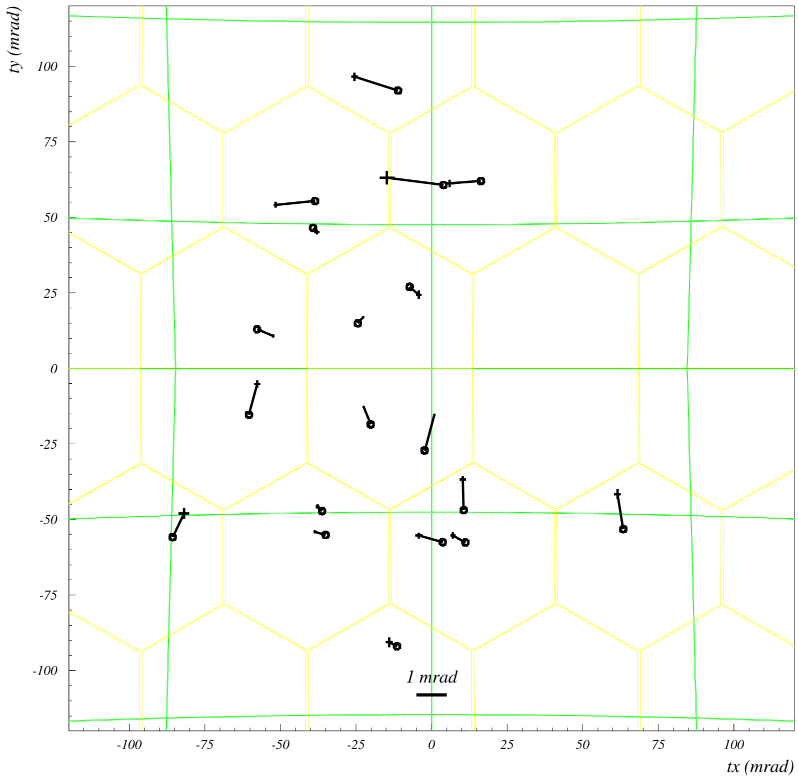

Figure 22: Alignment of the RICH relative to the calorimeter for the magnet on data, runs 5488 and 5490, target Inner I.

The same analysis was also performed on the data recorded with magnetic field. In this case, of course, only electrons that were produced in the region after the magnet correspond to straight tracks. Note, however, that for most of the detector solid angle the signal in the (φ_c, ϑ_c) histogram, Fig. 6, corresponding to these late conversions, is still strong enough not to be obscured by bent tracks. The analysis yields results that are very much consistent with the values deduced in the data without magnetic field, with the only exception in the area around the beam pipes (Figs. 22 and 23).

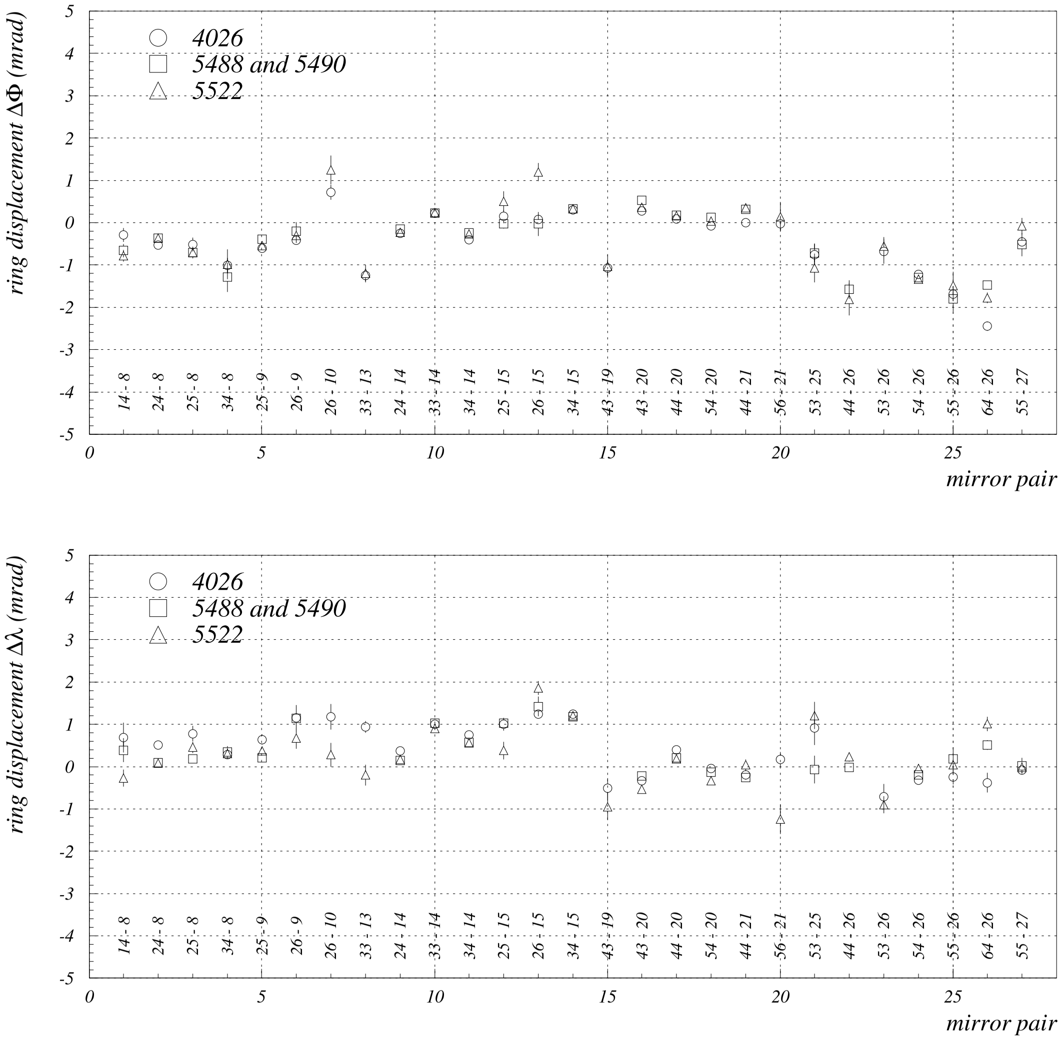

Figure 23: Comparison of results from magnet on data: displacement of each combination of spherical (first index) and planar (second index) mirror segments, run 4026 without magnetic field (circles), runs 5488 and 5490 with magnetic field, wire target Inner I (squares), run 5522 with magnetic field, two targets in Station I (triangles).

6 Summary

We summarize this report by observing that a method was developed for the relative alignment of the RICH and ECAL which uses recorded data. By applying the alignment parameters for each mirror segment as derived by this method, a significant improvement in the resolution in the Čerenkov angle measurement could be obtained.

The method was tested both on various sets of real data, recorded without magnetic field, as well as on simulated data. The method gives consistent results independent of the data set used. Given the limited statistics of simulated data small systematic biases cannot be completely excluded, but seem to be below the effects observed in the real data. We also note that the tests on data recorded with magnetic field indicate that the method can be used there as well, with some minor modifications in the regions close to the beam.

References

[1] A. Gorišek, Diploma thesis, University of Ljubljana, June 1997;
A. Gorišek, P. Križan, IJS Report, IJS-DP-7688, April 1997;
A. Gorišek et al., Nucl. Inst. and Meth. A433 (1999) 408-412.

[2] R. Pestotnik, P. Križan, S. Korpar and M. Starič, *Quality Test for the 98 RICH Common DAQ Data*, IJS Report, IJS-DP-8033, March 1999.

[3] P. Conde and D. Dujmić, *Quality Test for the 98 RICH Common DAQ Data*, HERA-B Note 99-015, February 1999.

[4] D. Dujmic, R. Eckmann and R.F. Schwitters, *Reconstruction of Photon Directions in the HERA-B RICH*, UT Report, December 1998.